Summanen, a new meteorite impact structure in Central Finland

Plado, Jüri

2018-11

Plado , J , Hietala , S , Kreitsmann , T , Lerssi , J , Nenonen , J & Pesonen , L J 2018 , ' Summanen, a new meteorite impact structure in Central Finland ' , Meteoritics and Planetary Science , vol. 53 , no. 11 , pp. 2413-2426 . https://doi.org/10.1111/maps.13134

http://hdl.handle.net/10138/321414
https://doi.org/10.1111/maps.13134

acceptedVersion

Summanen, a new meteorite impact structure in Central Finland

Jüri PLADO[1], Satu HIETALA[2], Timmu KREITSMANN[1], Jouni LERSSI[2], Jari NENONEN[2] and Lauri J. PESONEN[3]

[1]Department of Geology, University of Tartu, Ravila 14A, 50411 Tartu, Estonia

[2]Geological Survey of Finland, P.O. Box 1237, Neulaniementie 5, FI-70211 Kuopio, Finland

[3]Solid Earth Geophysics Laboratory, Physics Department, University of Helsinki, P.O. Box 64, Gustaf Hällströminkatu 2, FI-00014 Helsinki, Finland

Abstract-The Summanen structure (62°39.0'N, 25°22.5'E) is located within the Paleoproterozoic Central Finland Granite Belt, Fennoscandian Shield. The structure is hidden under Lake Summanen and not directly observable. It owes its discovery to low altitude airborne geophysical data, which revealed a circular, ~2.6 km wide electromagnetic in-phase, and resistivity, anomalies. Two field campaigns were conducted in 2017 to search for impact signatures. The field-work concentrated on the south-eastern side of the lake following the ice flow direction of the latest (Weichselian) glaciation. In addition, the islands and the SE peninsulas of the mainland were investigated for outcrops and glacial erratics. A few tens of erratic boulders with shatter cones and striated features, and a few brecciated rocks were discovered. Lamposaari Island in the eastern part of the lake revealed one fractured outcrop containing in-situ porphyritic granite with converging striated features. Microscopic shock metamorphic features in two shatter-cone-bearing samples of porphyritic granite were found. These are planar deformation features (PDFs; up to two sets) in quartz and kink bands in biotite. Based on these geological, geophysical, and petrographic results we suggest that Lake Summanen hides a relatively small, probably simple, meteorite impact structure, the twelfth confirmed one in Finland, of so far unknown age.

INTRODUCTION

Earth's impact record is incomplete when compared with other solid planetary bodies due to the dynamics of the terrestrial geology and to the fact that water covers much of the surface of our planet. This incompleteness is notable also when comparing different continental regions of Earth, as there is a pronounced concentration of known impact structures in some regions (e.g., North America, northern Europe, and Australia) and a dearth or lack thereof in others (such as Asia, South America and central Africa). The Fennoscandian Shield belongs to an area with high concentration, hosting about 10 % of the global record of confirmed meteorite impact structures. This high percentage is due to (i) the considerable ages of the rocks and their good and widespread preservation, (ii) scientific awareness, and (iii) dense geological and geophysical data coverage. Good preservation of crater structures is explainable by tectonic circumstances. The Fennoscandian Shield forms the north-westernmost part of the East European Craton, which forms the basement of Finland, north-western Russia, Norway, and Sweden. The crystalline rocks that make up the present shield have been formed during various accretional, rifting, and orogenic stages during the Archaean and Proterozoic. A long peneplanization period (since ~1.5 Ga) has led to the formation of a flat and stable environment, favorable for long-term survival of impact structures (Puura and Plado 2005). Pleistocene glaciers sculptured the Fennoscandian Shield, but their influence has been rather minor: glacial erosion over the entire shield was 200 m maximum (Lidmar-Bergström 1997). Erosion has, however, been selective by deepening features filled with easily disintegrated rocks, such as suevites and other breccias in impact structures. Another aspect that has contributed to the accumulation of a high number of proven impact craters is the awareness of professional geologists about the topic. The Nordic countries, including Finland, have had a long tradition of geological research. Systematic search for impact structures has been carried out since the 1980s (Henkel and Pesonen 1992), resulting in several new impact crater discoveries in the 1990s and 2000s (Abels et al. 2002; Deutsch 1998; Dypvik et al 2008).

BACKGROUND

The Summanen geophysical feature, which is centered at 62°39.0’N and 25°22.5’E (Fig. 1) was first identified in the early 2000’s by Jouko Vanne, a geologist at the Geological Survey of Finland (Lerssi et al. 2007). The observation was based on low altitude aeroelectromagnetic data that revealed circular electromagnetic in-phase component and apparent

resistivity anomalies (Fig. 2) associated with Lake Summanen. The anomalies are strikingly similar to the apparent resistivity anomaly that is associated with nearby (50 km south from Summanen; Fig. 1a) Lake Karikkoselkä (Lerssi et al. 2007, Pesonen et al. 1999), the impact origin of which was proven in 1996 (Lehtinen et al. 1996).

Two important observations must be emphasized. First, most of the central Finland lakes do not show such electromagnetic anomalies. Second, the observed anomalies at Karikkoselkä were proven not to be caused by the electrically conductive lake water nor by the Holocene bottom sediments, but rather by a lens of porous brecciated rock containing somewhat saline fluids (Pesonen et al. 1999).

Lake Summanen is located 9 km south-east of the nearest city, Saarijärvi, and 275 km north of Helsinki. It is elliptical (8 × 4 km) in shape, whereby the longest axis extends in NW-SE direction due to the erosional influence of the latest (Weichselian) glaciation. The area became deglaciated about 10,700 years ago (Stroeven et al. 2016). Presently, the water level of Lake Summanen is at 108.5 m a.s.l. The lake is connected to several other surrounding lakes. It also hosts two major islands, Summassaari and Lamposaari (Fig. 1b), which are offset from the central aeroelectromagnetic anomaly (Fig. 2).

Compared to the nearby lakes, Lake Summanen is relatively deep, with a maximum water depth of 41 m (Fig. 1b). The deep (>10 m) part of the lake coincides with the outline of the supposed crater, as derived from aeroelectromagnetic data. The deepest (>30 m) area is associated with the south-eastern side of the supposed crater, which is on the downrange side of the direction of advance (from about 295° to 115°) of the Weichselian ice sheet. Considering that the bathymetric depression and aeroelectromagnetic anomalies represent the crater outline, the most promising regions to find boulders from the lake depression are to the southeast of the lake: Lamposaari island and the areas on the southeastern coast of Lake Summanen (Fig. 1b).

The Central Finland Granitoid Complex (CFGC) hosts the Lake Summanen area. The complex has an Orosirian age (1.91-1.88 Ga) and covers an area of about 44,000 km^2 in central Finland. Predominant rocks are plutonic granites and granodiorites. Mafic rocks are sparse, and their composition is generally dioritic. Emplacement and deformation of these synorogenic rocks in central Finland relates to the accretion of two arc complexes during the Orosirian. A proposed (Nironen 2003, 2005) division classifies the rocks into syn-kinematic (1.89–1.87 Ga) and post-

kinematic (1.88–1.86 Ga) types, based on mineral composition, texture, and degree of deformation. Syn-kinematic plutons consist of I-type granodiorite and granite. Post-kinematic plutons are peraluminous and have a prominent sedimentary component in their source; they have A-type granite characteristics. Post-kinematic rocks are undeformed or slightly foliated plutons crosscutting the syn-kinematic rocks (Nironen et al. 2000). Post-kinematic plutons have been divided into three types according to their petrographic and mineral-chemical characteristics (Elliott et al. 1998, Nironen et al. 2000). Type 1 plutons are granodiorites and granites, Type 2 plutons are typically biotite±hornblende monzogranites, and Type 3 plutons are quartz monzonites and granites that contain pyroxene (Nironen et al. 2000).

Precambrian rocks of the Summanen area belong to the Type 2 plutons, the so-called Saarijärvi bimodal suite (Nironen 2003). Thus, the rocks of the Saarijärvi suite are not post-orogenic in the full sense of the word, as they represent the local extension during the main phase of the orogeny (Mikkola et al. 2016). Structurally, the Saarijärvi pluton is generally undeformed but may contain a weak magmatic foliation. Some lineaments crosscut the Saarijärvi pluton and exhibit zones of weak regional foliation with low-grade metamorphic mineral assemblages. The magmatic foliation was suggested (Nironen et al. 2000) to be due to deformation, possibly related to exhumation, which took place after the emplacement of the post-kinematic plutons. Zircon from Saarijärvi biotite-hornblende granite has been dated by the U-Pb technique to 1880 ±3 Ma (Rämö et al. 2001). Common textural observations for the CFGC granitoids are that they are even-grained and K-feldspar porphyritic. Country rocks in the Summanen and surrounding area are mainly porphyritic granites and leucogranites (Fig. 3a). The porphyritic granites have a phenocryst-supported cumulus fabric, whereby the phenocrysts are in contact with each other. The size of subhedral feldspar phenocrysts varies from 1 to 3 cm. In the southern part of Lake Summanen, granitoid rocks are syn-kinematic and slightly foliated, and they do not exhibit porphyritic texture.

Quaternary deposits within the Lake Summanen area consist of sandy basal till, silt, clay, gravel, sand, and peat deposits (Fig. 3b). Basal till was deposited during the deglaciation phase of the Weichselian glaciation (Rainio and Johansson 2004). The thickness of the basal till layer varies between 1 and 4 m (Kielosto and Lindroos 1984). About 10,700 years ago, a long southeast to northwest oriented esker ridge was deposited in the meltwater tunnel under the

glacier. The esker, consisting of gravel and sand, extends through Lake Summanen and is responsible for the arrowhead-like shape of Summassaari Island (Fig. 1b). When the Lake Summanen basin was uncovered from the continental ice, varved clay was deposited in the lake depression. Homogeneous lacustrine clay covers the varved clays. Some low areas around Lake Summanen are covered by silt, clay, and peat deposits (Lerssi et al. 2007).

GEOPHYSICAL CHARACTERISTICS

The regional (Saarijärvi quadrant, central Finland) aerogeophysical studies were carried out in 1995 by the Geological Survey of Finland. They included low-altitude (30-40 m) magnetic total field and electromagnetic measurements with a north-south flight direction and a line spacing of 200 m. The magnetic and electromagnetic data were registered four times per second, corresponding to about 12.5 m point spacings. The magnetic recording system included two optically pumped cesium magnetometers. The electromagnetic system applied a vertical coplanar broadside coil configuration, installed rigidly on wing tips, that operated at frequencies of 3125 and 14,368 Hz. All data were processed at the Geological Survey of Finland (Lerssi et al. 2007).

Lake Summanen is surrounded by strong (up to 1000 nT) regional magnetic anomalies with a general trend from the SW to the NE. The central part of the lake is characterized by weak magnetic relief, lacking any prominent anomalies (Fig. 2c). Such a pattern is not indicative for an impact origin, but is typical for many impact structures in Fennoscandia that lack highly magnetic impact melt rocks, such as, e.g., Jänisjärvi (Elo et al. 2000), Karikkoselkä (Pesonen et al. 1999), Suvasvesi South (Donadini et al. 2006), and Tvären (Ormö and Blomqvist 1996). Several reasons may contribute to the low gradients: (i) shock induced demagnetization (Bezaeva et al. 2016; Kohout et al. 2012; Louzada et al. 2011), (ii) post-impact oxidation of ferromagnetic minerals into less magnetic forms, e.g. oxidation of ferromagnetic magnetite to antiferromagnetic hematite, (iii) low magnetization of post-impact sediment infill and water, covering deeper, more magnetic rocks (see Pilkington and Grieve 1992), and (iv) random orientation of magnetization vectors in allochthonous crater-fill breccias.

In-phase aeroelectromagnetic data (Fig. 2b) over Lake Summanen reveal a strikingly circular anomaly about 2.6 km wide, which is related to the central part of the lake. The anomaly is distinct, as other nearby lakes lack such in-phase anomalies. The apparent resistivity map (Fig. 2b) shows an anomaly that is slightly wider compared to the in-phase component anomaly,

and is not as perfectly circular. Other strong and distinctly linear anomalies in the surroundings can be related to rural settlements and power lines.

The spatial resolution (2.5 × 2.5 km) of the available gravity measurements do not allow any conclusions to be drawn for the Summanen structure, as no measurements were made for the lake area. In late winter 2006, however, the lake was profiled from ice by using the electromagnetic multifrequency apparatus (SAMPO) of the Geological Survey of Finland. SAMPO is a wide-band electromagnetic system in which the transmitter is a horizontal loop on the ground/ice and the receiver measures the three perpendicular magnetic components of the electromagnetic field at 81 frequencies from 2 to 20,000 Hz (Soininen and Jokinen 1991). The transmitter and receiver were located on the profile 500 m apart, and the result was given to the central point of the system. Measurements were performed at every 200 m, but condensed to 50 m in the central parts of two perpendicular (SW-NE and NW-SE, respectively; Fig. 2) profiles. For qualitative interpretation, the SAMPO data measured at each frequency were transformed into curves of apparent resistivity as a function of depth using the algorithm of Aittoniemi et al. (1987). The curves were subsequently interpolated into apparent resistivity images (Fig. 4) by Lerssi et al (2007). An apparent resistivity value of 4500 Ωm was used for background. Bowl-shaped low resistivity features can be seen on both profiles (Fig. 4). Very low resistivities (<40 Ωm) are associated with Quaternary sediments. The rest of the bowl-shaped depression may be filled with low resistivity (from 40 to about 400 Ωm) sediments, or resistivities are lowered by fracturing of the basement.

METHODS FOR THIS INVESTIGATION

In summer 2017, we carried out two field campaigns to collect geological data, aiming to clarify the origin of the geophysical anomalies. Based on experiences from other impact case studies (e.g., Karikkoselkä, Keurusselkä, the Suvasvesi North and South, and Paasselkä), we searched for impact rocks occurring as in-situ outcrops and as erratic boulders. Erratic boulders with macroscopic shock deformation evidence were searched primarily to the south-east of the lake, corresponding to the ice-drift trend. Boulder findings were GPS-referenced, lithology was described, photographs were taken and hand samples collected. Seventeen thin sections were prepared from breccias and rocks containing shatter cone features.

Measurements of PDF orientations were done at the University of Tartu, Estonia, with a LOMO FS universal-stage (U-stage) mounted on a polarizing microscope. A standard technique described by Langenhorst (2002) was followed in measuring the orientation of the c-axis, and poles to PDFs relative to the orientation of the thin section. Results were analyzed using the ANIE (a mathematical algorithm for automated indexing of PDFs in quartz grains) program by Huber et al. (2011). In ANIE, 5° error and ranges of values were used for indexing.

RESULTS

Geological Observations

At the NW side of Lamposaari, the island located to the ESE of the center of the aerogeophysical anomalies, a solid outcrop was found (Fig. 5). The outcrop (observation No. 21 in Fig. 3c) is located ~400 m outside of the edge of the electromagnetic anomalies. The outcrop is about 6 m long, is elongated at 105-285˚, and exposes granites of different grain sizes: fine-grained granite in the eastern, and coarse-grained porphyritic granite in the western parts. The fine-grained granites contain converging striated features on slightly conical fracture surfaces (Fig. 5) and are more fractured compared to the porphyritic granites.

Eight glacially derived erratic boulders with shatter cones were found at the western shoreline of Lamposaari Island and on the mainland to the SE of the lake (Table 1). Our search concentrated on the lake's shoreline, forest roads and piles of rocks collected during deforesting activities. The reason for this is that rocks untouched by waves or human activity are covered by a thick layer of moss, making shatter-cone-bearing rocks difficult to find. During deforestation, the boulders are moved into piles within a distance of < 100 m from their glacially derived location. The erratic boulders in the area are generally well-rounded, but the carrying shatter cones are angular, suggesting a short travel distance. Most shatter cones were found within a distance of 5 km SE from the center of the geophysical anomalies (Fig. 3c). The outmost shatter-cone-bearing boulder was found at the distance of ~10 km from the anomalies (No. 11 in Fig. 3c and Table 1). Most of the cones are hosted by fine-grained granite (Figs. 6b, c, and e), but in rare cases, some have also formed in coarse-grained porphyritic granite (No. 29 in Fig. 3c and Table 1, Fig. 6d).

Mineralogical observations

Microscopically examined samples can be divided into three groups. First, there are monzogranites (Nos. 8, 25, and 31; Table 1) that are composed of quartz, feldspar, biotite, and amphibole. Accessory apatite and zircon are more abundant compared to the samples of the other groups. Hydrothermal alteration is pervasive and is mostly evidenced by sericitization of feldspar and chloritization of biotite and amphibole. Second, coarse-grained granites (Nos. 3, 4, and 24; Table 1) are composed of quartz, feldspar, and biotite. Samples SHHI-2017-4 and -24 are brecciated and composed of clasts of coarse-grained granite, whereas sample SHHI-2017-3 has microscopic veins, filled with mineral clasts from surrounding rock. In all three samples sericitization and perthitization of feldspar are common. Quartz and feldspar are occasionally fractured and coated with reddish Fe-hydroxide. Third, aplitic granites (Nos. 10, 11, and 21; Table 1) are composed of the same minerals as the coarse-grained granite, but the grain size is smaller and the rock is more even-grained. Feldspar is occasionally altered and coated with Fe-hydroxides. Samples SHHI-2017-10 and -11 represent monomict breccia.

Shock petrography

In two shatter-cone-bearing samples (SHHI-2017-3 and -8; Fig. 7 and Table 1) planar deformation features (PDFs) were identified. Altogether sixty four (fifty seven in SHHI-2017-3 and seven in SHHI-2017-8) measurements of the angles between host quartz c-axes and poles to PDFs were made in 60 quartz grains. In most cases, there was one set of PDFs per grain, usually penetrating the entire grain (Figs. 7 and 8). As it is impossible to measure the exact position of a-axes in quartz grains under the U-stage, at least two sets of PDFs - not including the (0001) orientation - are needed for unambiguous indexing (Losiak et al. 2016). Thus, we avoided indexing PDFs if the second set was not present. The angles between c-axis and poles to PDF are shown in Fig. 8. Eighty three percent of the measured angles are between 20-35°, which with 5° error would correspond to $\{10\bar{1}3\}$ (22.95°) or $\{10\bar{1}2\}$ (32.42°) in most cases. No PDFs with basal (0001) orientation were identified.

The indexed orientations of four grains with two sets of PDFs (e.g., Fig. 7c) were $\{10\bar{1}3\}$-$\{11\bar{2}2\}$, $\{10\bar{1}4\}$-$\{3\bar{1}\bar{4}1\}$, $\{10\bar{1}4\}$-$\{10\bar{1}2\}$, and $\{10\bar{1}3\}$-$\{2\bar{1}\bar{3}1\}$. All PDFs are decorated. Average spacings between neighboring features are between 5 and 8 μm. In addition to PDFs, planar fractures (PF) are common, and in rare cases, feather features (FF) (Fig. 9c). Kink bands in

biotite (Fig. 9b) are abundant, including in the samples in which quartz does not display shock metamorphic features (e.g. sample KS2, No. 31 in Table 1). Kink bands are not uniquely associated with impact-related shock metamorphism and can form *via* endogenic processes. However, as the target rock has experienced only low grade metamorphism and most of the microscopically analyzed samples were shatter cones, it is likely that kink banding in biotite our samples is due to shock metamorphism. In sample SHHI-2017-8 (No. 8 in Table 1) one zircon grain with possible planar features was found (Fig. 9d).

DISCUSSION

Two types of diagnostic evidence of hypervelocity impact were found in the Lake Summanen area: shatter cones and PDFs in quartz. Shatter cones form at shock pressures in the range of 2–30 GPa (e.g. French and Koeberl 2010; Baratoux and Reimold 2016). According to Baratoux and Reimold (2016), the discrimination of shatter cones from other geological features (e.g. slickenslides, plumose fractures, crenulation cleavage) can be made based on several macroscopic features. The features include distribution of striated surfaces, lithology, shape, amplitudes, orientation, and morphology of striations. The shape of striated surfaces should be curved and the orientation of striated surfaces variable. Striations must diverge, and morphology should be rounded. The amplitude of the striations (the difference in height between the ridges and the grooves in relation to the average surface area of the stone) is smaller than its wavelength (the distance between adjacent ridges or grooves), usually >1mm.

Shatter cones in Summanen match these requirements positively. The surfaces are curved, conical, the orientation of striations is variable, and they diverge from the apex, and striations are pervasive. Some striations on the surface show negative (concave) cone structure. The apical angles vary between 45° and 75°. The best developed shatter cones occur in altered and fine grained aplitic granite. At present, all shatter cones were in found in boulders of post-kinematic granitoid. Based on the thin section determination, the modal amount of quartz is low. Thus, the target rock is more likely closer to a quartz monzonite than a granite (see Elliot 2001).

PDFs are the most commonly used diagnostic features for identifying impact structures (e.g., Ferrière et al. 2009; French and Koeberl 2010). PDFs occur as single or multiple sets of parallel, planar optical discontinuities, oriented along crystallographic planes that are sometimes resolvable by the optical microscope as thin (30 to 200 nm) lamellae, or as planes decorated with

tiny vugs (so-called decorated PDFs; Grieve et al. 1996). Decorated PDFs are defined as PDFs produced from non-decorated PDFs by secondary annealing. The spacing of PDFs can vary within one set from 2 to 10 μm (Stöffler and Langenhorst 1994). In Summanen, PDFs were found in samples SHHI-2017-3 and -8 (Table 1). Both of these are shatter-cone-bearing samples. PDFs in shatter-cone-carrying samples have been described by different authors (Dressler 1990; Fackelman et al. 2008; Ferrière et al. 2010; Hasch et al. 2016; and Zaag et al. 2016). In the nearby Keurusselkä impact structure (Fig. 1a), Hasch et al. (2016) found PDFs in three shatter-cone-bearing samples from the central part of the structure. Similarly to our results, two sets of PDFs were rare and the amount of (0001) indexed PDFs was surprisingly small. On the other hand, Ferrière et al. (2010) described up to three to five sets of PDFs in shatter-cone-bearing samples from Keurusselkä. This shows that the presence of PDFs in shatter-cone-bearing rocks can be variable. Hasch et al. (2016) argued that most of the PDFs form close to the shatter cone surface. Thus, the orientation and proximity of the thin section relative to the shatter-cone surface could be an important factor controlling the abundance of PDFs found.

PDFs can be used to estimate average shock pressures from impact (Grieve et al. 1996). In a simplified view, the abundance of (0001), $\{10\bar{1}3\}$, and $\{10\bar{1}2\}$ orientations are used. When PFs and (0001) orientation are most common, the grain is very weakly shocked. If $\{10\bar{1}3\}$ is the most common, with rare (0001), then it is weakly to moderately shocked. The increase in the $\{10\bar{1}2\}$ abundance also suggests increase in the experienced pressures. Thus, quartz grains with mostly $\{10\bar{1}3\}$ and $\{10\bar{1}2\}$ orientation have experienced pressures >20 GPa. In our samples we did not find (0001) orientation, and the angles between the c-axes and poles to PDF suggest that the most common orientations are $\{10\bar{1}3\}$ and the second-most common is $\{10\bar{1}2\}$. This indicates that the samples are at least moderately to strongly shocked, and the pressures had to have been more than 15 GPa. This is supported by the fact that most of the PDFs penetrate the entire grain, which is thought to indicate that they are formed at shock pressures at the higher end of the PDF formation regime (Stöffler and Langenhorst 1994, Zaag et al. 2016). On the other hand, more than one set of PDFs is rare, contradicting the higher shock pressures. If that was the case, multiple sets of PDFs would be common in one grain (Stöffler and Langenhorst 1994). Further studies are needed to constrain the pressure regime better.

The aeroelectromagnetic data show that the Summanen structure has a diameter of about 2.6 km. Considering partial erosion of the structure, the original diameter of the crater may have been larger. However, we do not know when the impact occurred. Therefore, we are unable to estimate the rate of erosion and the original diameter. As the structure is small, presumably of simple, bowl-shaped geometry, and has survived erosion, we tentatively lean towards the Phanerozoic, most likely a late Paleozoic to Cenozoic age.

CONCLUSIONS

The Summanen impact structure in central Finland, located in a Paleoproterozoic granitic terrain of the Fennoscandian Shield, was discovered due to pronounced aeroelectromagnetic anomalies. The anomalies coincide with the central part of Lake Summanen and are circular, unlike the lake's shoreline that was sculptured by the Weichselian glaciation. Moreover, these anomalies are significantly stronger compared to those in nearby lakes of the region and are strikingly similar to those corresponding to the Lake Karikkoselkä impact structure.

The identification of shatter cones in glacially derived erratic boulders, and multiple sets of planar deformation features in quartz prove that the structure is of impact origin. The Summanen structure is the twelfth confirmed impact structure in Finland.

Acknowledgments--M. Lingadevaru and Mohd. Aslam (Central University of Karnataka, India) are acknowledged for their assistance in the field. Juho Kirs contributed to the study with helpful discussions. We thank Auriol Rae and an anonymous reviewer for their constructive reviews, and Uwe Reimold for the editorial handling. Grant # IUT20-34 by the Estonian Research Council provided support for this study.

REFERENCES

Abels A., Plado J., Pesonen L.J., and Lehtinen M. 2002. The impact cratering record of Fennoscandia – A new look at the database. In *Impacts in Precambrian Shields*, edited by Plado J. and Pesonen L.J. Berlin: Springer-Verlag. pp. 1-58.

Aittoniemi K., Rajala J., and Sarvas J. 1987. Interactive inversion algorithm and apparent resistivity versus depth (ARD) plot in multifrequency depth soundings. *Acta Polytechnica Scandinavica Applied Physics Series* 157:1-34.

Baratoux D. and Reimold W.U. 2016. The current state of knowledge about shatter cones: Introduction to the special issue. *Meteoritics & Planetary Science* 51:1389-1434.

Bezaeva N.S., Chareev D.A., Rochette P., Kars M., Gattacceca J., Feinberg J.M., Sadykov R.A., Kuzina D.M., and Axenov S.N. 2016. Magnetic characterization of non-ideal single-domain monoclinic pyrrhotite and its demagnetization under hydrostatic pressure up to 2 GPa with implications for impact demagnetization. *Physics of the Earth and Planetary Interiors* 257:79-90.

Deutsch A. 1998. New pathfinders to impact structures: The Finnish way. *Meteoritics & Planetary Science* 33:3.

Donadini F., Plado J., Werner S.C., Salminen J., Pesonen L.J., and Lehtinen M. 2006. New Evidence for Impact from the Suvasvesi South Structure, Central East Finland. In *Biological Processes Associated with Impact Events*, edited by Cockell C., Koeberl C., and Gilmour I. Berlin: Springer-Verlag. pp. 287-307.

Dressler B. 1990. Shock metamorphic features and their zoning and orientation in the Precambrian rocks of the Manicouagan Structure, Quebec, Canada. *Tectonophysics* 171: 229–245.

Dypvik H., Plado J., Heinberg C., Håkansson E., Pesonen L.J., Schmitz B., and Raiskila S. 2008. Impact structures and events—A Nordic perspective. *Episodes* 31:107–114.

Elliott B.A., Rämö O.T., and Nironen M. 1998. Mineral chemistry constraints on the evolution of the 1.88-1.87 Ga post-kinematic granite plutons in the central Finland granitoid complex. *Lithos* 45:109–129.

Elo S., Zhdanova L., Chepik A., Pesonen L.J., Philippov N., and Shelemotov A. 2000. Comparative geophysical description and modelling of Lappajärvi and Jänisjärvi impact structures, Fennoscandian shield (abstract). In: *Meteorite Impacts in Precambrian Shields, Programme and Abstracts of ESF workshop*, edited by Plado J. and Pesonen L.J. Geological Survey of Finland and University of Helsinki, Espoo. p. 35.

Ferrière L., Morrow J.R., Amgaa T., and Koeberl, C. 2009. Systematic study of universal-stage measurements of planar deformation features in shocked quartz: Implications for statistical significance and representation of results. *Meteoritics & Planetary Science* 44:925–940.

Ferrière L., Raiskila S., Osinski G.R., Pesonen L.J., and Lehtinen M. 2010. The Keurusselkä impact structure, Finland—Impact origin confirmed by characterization of planar deformation features in quartz grains. *Meteoritics & Planetary Science* 45:434–446.

French B.M. and Koeberl C. 2010. The convincing identification of terrestrial meteorite impact structures: What works, what doesn't, and why. *Earth-Sciences Reviews* 98:123-170.

Hasch M., Reimold W.U., Raschke U., and Zaag P.T. 2016. Shatter cones at the Keurusselkä impact structure and their relation to local jointing. *Meteoritics & Planetary Science* 51:1534–1552.

Henkel H. and Pesonen L.J. 1992. Impact craters and craterform structures in Fennoscandia. *Tectonophysics* 216:31-40.

Huber M., Ferrière L., Losiak A., and Koeberl C. 2011. ANIE: A mathematical algorithm for automated indexing of planar deformation features in quartz grains. *Meteoritics & Planetary Science* 46:1418–1424.

Kielosto S. and Lindroos P. 1984. *Explanation for Quaternary map 1: 20 000, 2244 07 Saarijärvi.* Geological Survey of Finland.

Kohout T., Pesonen L.J., Deutsch A., Wünneman K., Nowka D., Hornemann U., and Heikinheimo E. 2012. Shock experiments in range of 10-45 GPa with small multidomain magnetite in porous targets. *Meteoritics & Planetary Science* 47:1671-1680.

Langenhorst F., 2002. Shock metamorphism of some minerals: Basic introduction and microstructural observations. *Bulletin of the Czech Geological Survey* 77:265–282.

Lehtinen M., Pesonen L.J., Puranen R., and Deutsch A. 1996. Karikkoselkä – a new impact structure in Finland. *LPSC abstracts*, XXVII:739-740.

Lerssi J., Mursu J., Niskanen M., and Pajunen H. 2007. *Summasjärven johtavuusanomalian tutkimukset vuosina 2005 ja 2006. Report Q19/2243,2244/2007/1*. Kuopio: Geological Survey of Finland 28 p. In Finnish.

Lidmar-Bergström K. 1997. A long-term perspective on glacial erosion. *Earth Surface Processes and Landforms* 22:297-306.

Losiak A., Golebiowska L., Ferrière L., Wojciechowski J., Huber M.S., and Koeberl C. 2016. WIP: A Web-based program for indexing planar features in quartz grains and its usage. *Meteoritics & Planetary Science* 51:647-662.

Louzada K.L., Stewart S.T., Weiss B.P., Gattacceca J., Lillis R.J., and Halekas J.S. 2011. Impact demagnetization of the Martian crust: Current knowledge and future directions. *Earth and Planetary Science Letters* 305:257-269.

Mikkola P., Heilimo E., Aatos S., Ahven M., Eskelinen J., Halonen S., Hartikainen A., Kallio V., Kousa J., Luukas J., Makkonen H.,Mönkäre K., Niemi S., Nousiainen M., Romu I., and Solismaa S. 2016. *Bedrock of the Jyväskylä area*. Espoo: Geological Survey of Finland, Report of Investigation, 227, 95 p.

Nironen M. 2003. *Central Finland Granitoid Gomplex – Explanation to the bedrock map.* Geological Survey of Finland. Report of Investigation, 157, 1–45.

Nironen M. 2005. Proterozoic orogenic granitoid rocks. In *Precambrian Geology of Finland – Key to the Evolution of the Fennoscandian Shield*, edited by Lehtinen M., Nurmi P.A., and Rämö O.T. Amsterdam: Elsevier B.V., 443–480.

Nironen M., Elliott B. A., and Rämö O. T. 2000. 1.88-1.87 Ga post-kinematic intrusions of the Central Finland Granitoid Complex: a shift from C-type to A-type magmatism during lithospheric convergence. *Lithos* 53:37–58.

Ormö J. and Blomqvist G. 1996. Magnetic modelling as a tool in the evaluation of impact structures, with special reference to the Tvären Bay impact crater, SE Sweden. *Tectonophysics* 262:291-300.

Pesonen L.J., Elo S., Lehtinen M., Jokinen T., Puranen R., and Kivekäs L. 1999. Lake Karikkoselkä impact structure, central Finland: New geophysical and petrographic results. Geological Society of America Special Paper 339, 131-147.

Pilkington M. and Grieve R.A.F. 1992. The geophysical signature of terrestrial impact craters. Reviews of Geophysics, 30, 161-181.

Pirttijärvi M. 1995. *TRANSAEM, Fortran-77 ohjelma GTK:n sähkömagneettisen lentomittausaineiston muuntamiseksi näennäiseksi johtavuudeksi ja syvyydeksi.* Geological Survey of Finland, internal report Q17.9/95/1.I In Finnish.

Puura V. and Plado J. 2005. Settings of meteorite impact structures in the Svecofennian crustal domain. In *Impact Tectonics*, edited by Koeberl C. and Henkel H. Berlin: Springer-Verlag. pp. 211-245.

Rainio H. and Johansson P. 2004. Jäätikkö sulaa. In *Jääkaudet*, edited by Koivisto, M. Helsinki: WSOY. pp. 69-86. In Finnish.

Rämö O.T., Vaasjoki M., Mänttäri I., Elliott B.A., and Nironen M. 2001. Petrogenesis of the post-kinematic magmatism of the central Finland Granitoid Complex I; radiogenic isotope constraints and implications for crustal evolution. *Journal of Petrology* 42:1971–1993.

Soininen H. and Jokinen T. 1991. *SAMPO, a new wide-band electromagnetic system.* Technical Programme and Abstracts, EAEG 53rd Meeting and Technical Exhibition, Florence, Italy, 26–30 May, 1991, 366–367.

Stöffler D. and Langenhorst F. 1994. Shock metamorphism of quartz in nature and experiment: I. Basic observation and theory. *Meteoritics* 29:155–181.

Stroeven A.P., Hättestrand C., Kleman J., Heyman J., Fabel D., Fredin O., Goodfellow B.W., Harbor J.M., Jansen J.D., Olsen L., Caffee M.W., Fink D., Lundqvist J., Rosqvist G.C., Strömberg B., and Jansson K.N. 2016. Declaciation of Fennoscandia. *Quaternary Science Reviews* 147:91-121.

Wait J.R. 1982. Chapter 3, Electromagnetic induction and loop–loop coupling. *Geo-Electromagnetism*. New York City: Academic Press.

FIGURE CAPTIONS

Fig. 1. (a) Location of the Summanen structure and the entire meteorite impact crater population in Finland. Symbol sizes are scaled to diameters of craters, but are exaggerated by about two times. (b) Topographic and bathymetric shaded relief map of the Lake Summanen area. The red line outlines Lake Summanen at the average water level of 108.5 m a.s.l. Maximum and minimum elevation levels are 231 and 67 m a.s.l., respectively. The maximum depth of the lake is 41 m. The dashed ring with a diameter of ~2.6 km indicates the outline of the proposed crater structure as derived from aeroelectromagnetic data (Fig. 2).

Fig. 2. (a) Aeromagnetic and aeroelectromagnetic (b) in-phase component and (c) apparent resistivity anomaly maps of the Lake Summanen area. A dashed ring with diameter of ~2.6 km indicates the interpreted outline of the anomaly within Lake Summanen. The apparent resistivity data in (c) were calculated from the in-phase and quadrature components using a half-space model (Pirttijärvi 1995; Wait 1982).

Fig. 3. Geological maps of (a) Svecofennian bedrock and (b) Quaternary sediments. (c) Locations of findings related to the Summanen structure. Numbers refer to descriptions of samples given in Table 1. Dashed ring with a diameter of ~2.6 km indicates the interpreted outline of the aeroelectromagnetic anomalies (Figs. 2b and c).

Fig. 4. Apparent resistivity models based on the wideband SAMPO electromagnetic measurements from ice of Lake Summanen (Lerssi et al. 2007). Black dots indicate locations of the original measurements (mid-points of the SAMPO system). X shows the location where the two profiles cross. Locations of the profiles are given in Fig. 2.

Fig. 5. Photos of the Lamposaari Island granite outcrop (No. 21 in Fig. 3c). Photo (a) shows converging striated features on a slightly conical fracture surface on the fine-grained granite.

Fig. 6. (a-c, e) Photos of shatter cone samples and (d) curved striations. (a) No. 1 (sample SHHI-2017-1), (b) No. 22 (sample SHHI-2017-22), (c) No. 3 (erratic boulder 3), (d) No. 29 (sample SU17-5), and (e) No. 3 (sample SHHI-2017-3). See Fig. 3c for locations and Table 1 for descriptions.

Fig. 7. Thin section microphotographs of PDFs, taken in cross polarized light. Orientation of PDFs is accentuated with the short red line. (a) Two quartz grains with one set of PDFs each, sample SHHI-2017-3 (No. 3, thin section 170353), (b) one set of PDFs in quartz, sample SHHI-2017-3 (170351). (c) two sets of PDFs of $\{10\bar{1}4\}$ and $\{10\bar{1}2\}$ orientations in quartz, sample SHHI-2017-8 (No. 8, thin section 170369), and (d) one set of PDFs in quartz, sample SHHI-2017-3 (170351). (e) One set of PDFs and PFs (orientation accentuated with the short blue line) in fragmented quartz aggregate. Yellow box highlights the area of the image (f), sample SHHI-2017-3 (170352), (f) one set of decorated PDFs, sample SHHI-2017-3 (170352). See Table 1 and Fig. 3c for descriptions and locations of samples.

Fig. 8. Histogram of angles between c-axis and poles to PDF's in 5° bins and possibly corresponding PDF orientations.

Fig. 9. Thin section microphotographs of possible shock deformation features, all images taken with crossed polarizers. (a) Brecciated vein in coarse-grained granite sample SHHI-2017-3 (No. 3, thin section 170353). Vein is filled with angular clasts of the minerals occurring in the surroundings (quartz and feldspar), (b) kink-bands in biotite, sample SHHI-2017-8 (No. 8, thin section 170369), (c) planar features and feather features in quartz, sample SHHI-2017-8 (thin section 170572), (d) possible planar microdeformations in zircon, sample SHHI-2017-8 (thin section 170571). Orientations of planar features are accentuated with short red lines. Abbreviations: Bt – biotite, Q – quartz, Kfs – potassium feldspar, PF – planar features, FF – feather features. See Table 1 and Fig. 3c for descriptions and locations of samples.

Table 1. Petrographic descriptions of samples from the Lake Summanen area.

Sample (numbers refer to locations on Fig. 3c)	Thin sections	**Shock** and possibly related features	Description
No. 1 Sample SHHI-2017-1 62°37'16.7''N 25°25'15.1''E		**Shatter cone**	Aplitic granite boulder with large shatter cone, 1.0×0.6 m in size. The boulder includes well preserved conical and diverging striations. Striations are distributed throughout the volume of the sample. Orientations of striations are variable, the apex angle is 40°.
No. 3 Sample SHHI-2017-3 62°37'21.0''N 25°25'16.2''E	170351 170352 170353	**Shatter cone** **PDFs in quartz, in up to**	Coarse-grained porphyritic granite boulder, 0.1×0.8×1.5 m in size. The boulder includes curved fracture surfaces of various orientations. Fracture surfaces are distributed throughout the sample. Striations are rounded and diverging. Microscopically the boulder comprises quartz, feldspar, and

Figs. 7a, b, d-f Fig. 9a		**2 sets per host grain**	to a lesser extent biotite. Shock-metamorphic features are common in quartz and include up to two sets of decorated PDFs, fractured quartz crystals, planar features (PF), and undulatory extinction. Most of the quartz grains with PDFs have reddish rims and exhibit slightly darker/yellow interference color compared to unshocked quartz grains.
No. 4 Sample SHHI-2017-4 62°37’27.3’’N 25°26’47.4’’E	170368	Kink bands in biotite - rare	Coarse-grained porphyritic granite boulder, 0.6×0.5×0.3 m in size. It shows concave fracturing with striations. The ridges and grooves are weakly curved. Microscopically, the sample represents a monomict granite breccia that is composed of quartz, feldspar, and biotite. Grains are angular and poorly sorted, with a bimodal grain size distribution. There is a cryptocrystalline groundmass of the same minerals. Quartz shows no indication of shock-metamorphism. Biotite has rare kink bands.
No. 8 SHHI-2017-8 62°35’52.7’’N 25°28’12.5’’E Fig. 7c Fig 9b-d	170369 170571 170572	**PDFs up to 2 sets per host grain,** feather features (FF)	Coarse-grained porphyritic monzogranite boulder, 0.4×0.3×0.3 m in size. The surface of the rock shows striations of 2 different directions. Striations are slightly curved. Microscopically the rock is composed of feldspar, amphibole, biotite, and quartz. In addition, there are chlorite after biotite and opaque minerals that are mostly associated with chlorite and amphibole. The latter two are alteration products. Accessory apatite, zircon and epidote crystals can be seen. Kink bands are common in biotite. Quartz grains are fractured and contain PFs, FFs, and up to two sets of PDFs.
No. 10 SHHI-2017-10 62°35’11.5’’N 25°28’14.2’’E	170490 170491	-	Decimeter-sized boulder of brittle, brecciated granite aplite from a hummocky moraine. Microscopically the sample is revealed as monomict breccia composed of angular clasts of aplitic granite. Granite clasts are made of quartz, feldspar, and rare biotite. Matrix is composed of small clasts of the same phases and cryptocrystalline masses of hematite/Fe-hydroxides. Quartz does not exhibit shock metamorphic features.
No. 11 SHHI-2017-11 62°34’34.7’’N 25°29’10.7’’E	170492	**Shatter cone**	Shatter cone on aplitic granite boulder with narrow hematitic crosscutting veins. The boulder is 0.3×0.4×0.2 m in size. Striations are diverging, morphologically rounded. The apical angle of the cone is 55°. Microscopically it was found that the granite is composed mostly of fine grained quartz and larger feldspar crystals and rare chloritized biotite. Feldspars are altered and often coated with cryptocrystalline hematite/iron hydroxides that are also common in fractures. Quartz clasts can be found in fractures but show no shock metamorphism.
No. 12 SHHI-2017-12 62°38’9.6’’N 25°26’13.33’’E		**Shatter cone**	Coarse-grained, porphyritic granite, 0.5×0.4×0.3 m in size, with conical, curved shatter cone surface. Striations are diverging and penetrative.
No. 20 SHHI-2017-20 62°37’48.7’’N 25°24’52.6’’E	-	**Shatter cone**	Erratic porphyritic granite boulder, 15×10×5 cm in size, representing a fragment of a bigger shatter cone with a curved fracture surface with a conical angle of 75°. Amplitudes of striations are at the mm scale, striations are

			rounded and diverging.
No. 21 SHHI-2017-21 LS1 62°38’46.1’’N 25°24’7.8’’E	170493 170570		Porphyritic aplitic granite from the outcrop with curved striated features. Microscopically, it is a fine-grained granite (thin section # 170493), composed of small quartz crystals (100-200 μm), larger (up to 1 mm) feldspar phenocrysts, and rare muscovite. Quartz shows no indication of shock metamorphism. Thin section # 170570 is composed of quartz, feldspar, and rare biotite. There is no indication to shock metamorphism at the microscopic level.
No. 22 SHHI-2017-22 62°38’45.76’’N 25°24’2.37’’E Fig. 6b		**Shatter cone**	Boulder of fine-grained porphyritic granite shatter cone, 0.4×0.4×0.2 m in size. Boulder is covered with oxides of manganese and iron. Shatter cone surface shows striations in 3 different directions. Striations are diverging and distributed throughout the volume of the sample. Striation shape is conical, and the apical angle is 45°. The amplitude of striations is up to 3 mm.
No. 24 SHHI-2017-24 62°38’5.17’’N 25°26’28.31’’E	170565 170566	Breccia	Boulder of brecciated, coarse-grained porphyritic granitoid. Microscopically this monomict granite breccia is composed of mostly quartz, feldspar, and minor biotite.
No. 25 SHHI-2017-25 62°38’9.98’’N 25°26’13.74’’E	170567 170568	**Shatter cone**	Monzogranite, composed mostly of quartz, feldspar, biotite, and secondary chlorite after amphibole. No shock metamorphic features were identified by microscopy. There is indication of hydrothermal alteration suggested by sericitization of feldspar.
No 29 Sample SU17-5 62°37’16.7’’N 25°25’15.1’’E	-	**Shatter cone**	Boulder of coarse-grained porphyritic granite, 20×15×10 cm in size. The sample includes both curved and planar fracture surfaces in four variable orientations. Fracture surfaces are distributed throughout the volume of the sample. Striations are rounded and slightly diverging.
No. 31 KS2 62°38’57.84’’N 25°20’0.24’’E	170569	Kink bands in biotite	Monzogranite boulder composed of quartz, feldspar, amphibole, biotite, accessory apatite and secondary chlorite after amphibole and biotite. The latter and altered feldspar hint at hydrothermal alteration. Quartz may carry fractures that are usually filled with chlorite. Planar features in quartz were not identified, but kink bands in biotite are common.

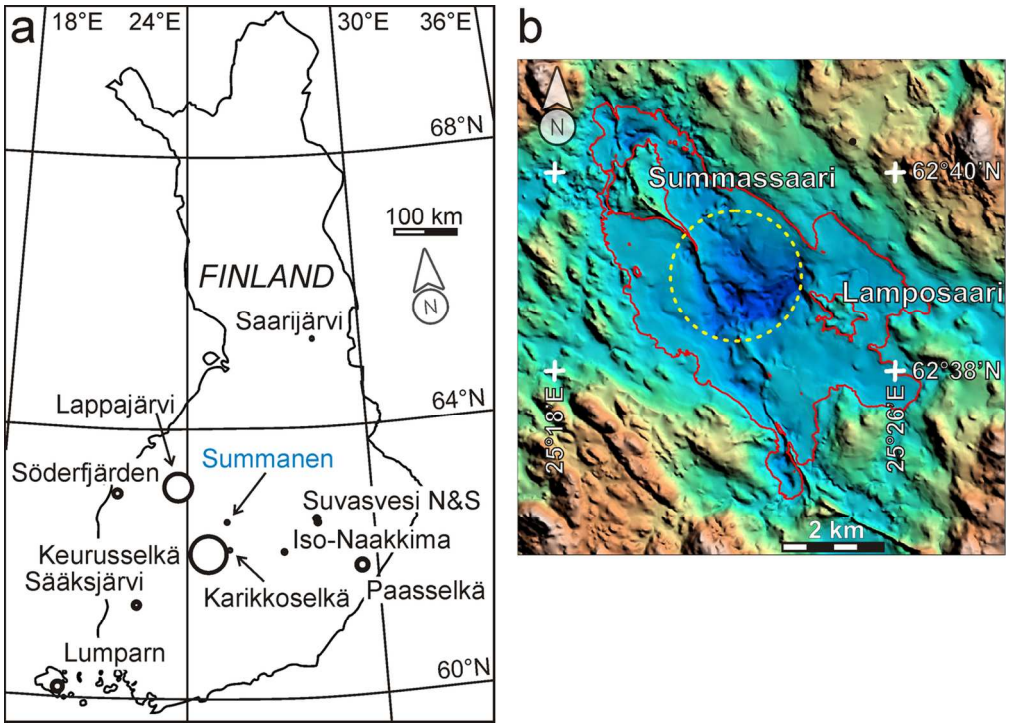

Fig. 1. (a) Location of the Summanen structure and the entire meteorite impact crater population in Finland. Symbol sizes are scaled to diameters of craters, but are exaggerated by about two times. (b) Topographic and bathymetric shaded relief map of the Lake Summanen area. The red line outlines Lake Summanen at the average water level of 108.5 m a.s.l. Maximum and minimum elevation levels are 231 and 67 m a.s.l., respectively. The maximum depth of the lake is 41 m. The dashed ring with a diameter of ~2.6 km indicates the outline of the proposed crater structure as derived from aeroelectromagnetic data (Fig. 2).

127x91mm (300 x 300 DPI)

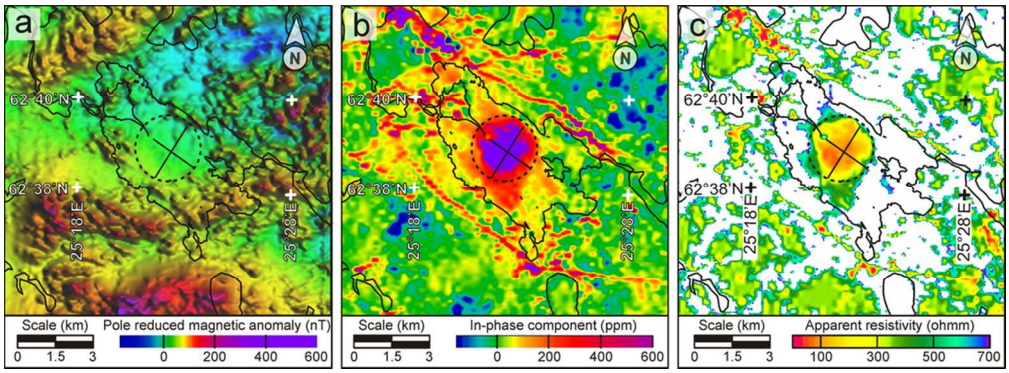

Fig. 2. (a) Aeromagnetic and aeroelectromagnetic (b) in-phase component and (c) apparent resistivity anomaly maps of the Lake Summanen area. A dashed ring with diameter of ~2.6 km indicates the interpreted outline of the anomaly within Lake Summanen. The apparent resistivity data in (c) were calculated from the in-phase and quadrature components using a half-space model (Pirttijärvi 1995; Wait 1982).

92x33mm (300 x 300 DPI)

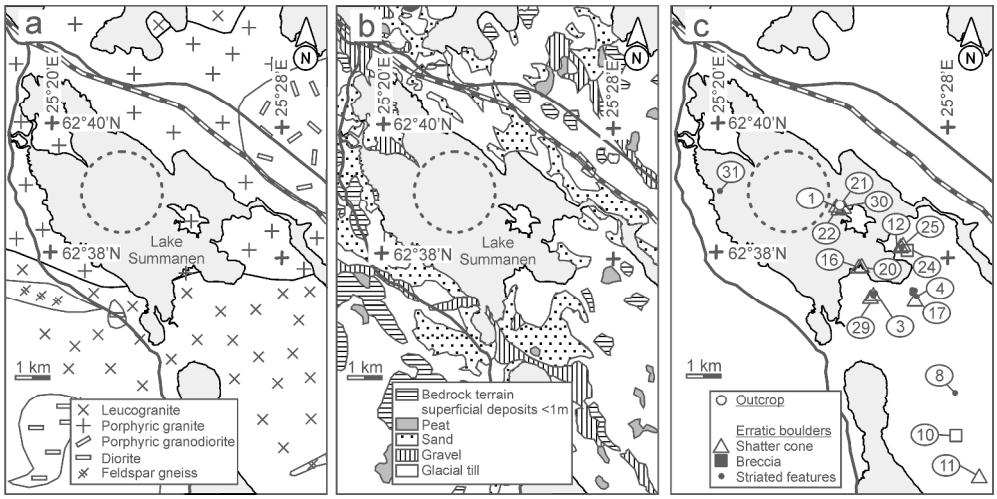

Fig. 3. Geological maps of (a) Svecofennian bedrock and (b) Quaternary sediments. (c) Locations of findings related to the Summanen structure. Numbers refer to descriptions of samples given in Table 1. Dashed ring with a diameter of ~2.6 km indicates the interpreted outline of the aeroelectromagnetic anomalies (Figs. 2b and c).

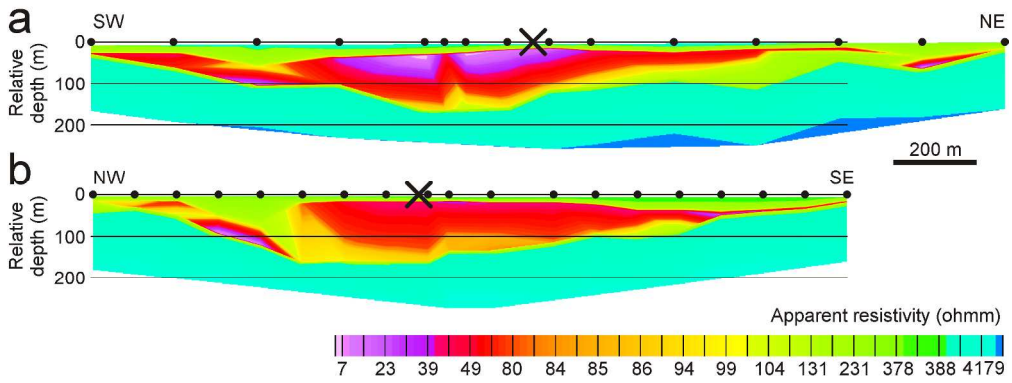

Fig. 4. Apparent resistivity models based on the wideband SAMPO electromagnetic measurements from ice of Lake Summanen (Lerssi et al. 2007). Black dots indicate locations of the original measurements (mid-points of the SAMPO system). X shows the location where the two profiles cross. Locations of the profiles are given in Fig. 2.

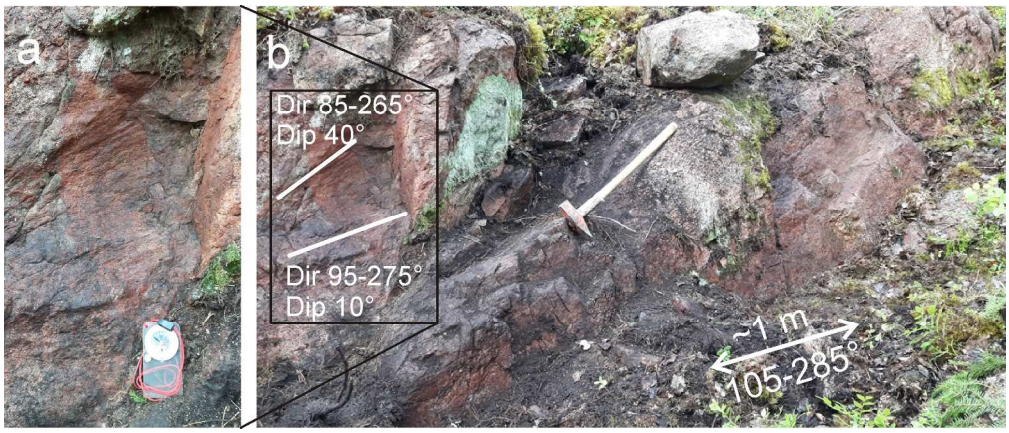

Fig. 5. Photos of the Lamposaari Island granite outcrop (No. 21 in Fig. 3c). Photo (a) shows converging striated features on a slightly conical fracture surface on the fine-grained granite.

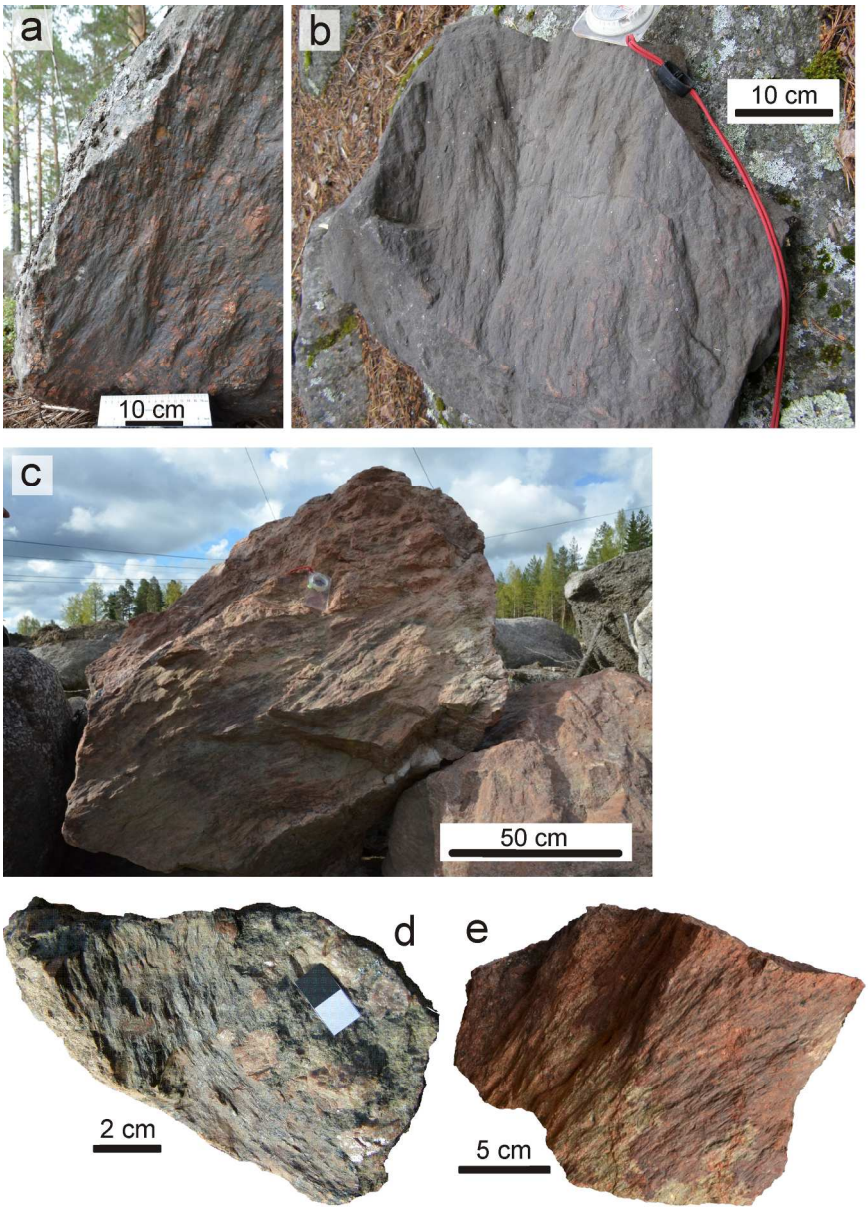

Fig. 6. (a-c, e) Photos of shatter cone samples and (d) curved striations. (a) No. 1 (sample SHHI-2017-1), (b) No. 22 (sample SHHI-2017-22), (c) No. 3 (erratic boulder 3), (d) No. 29 (sample SU17-5), and (e) No. 3 (sample SHHI-2017-3). See Fig. 3c for locations and Table 1 for descriptions.

228x316mm (300 x 300 DPI)

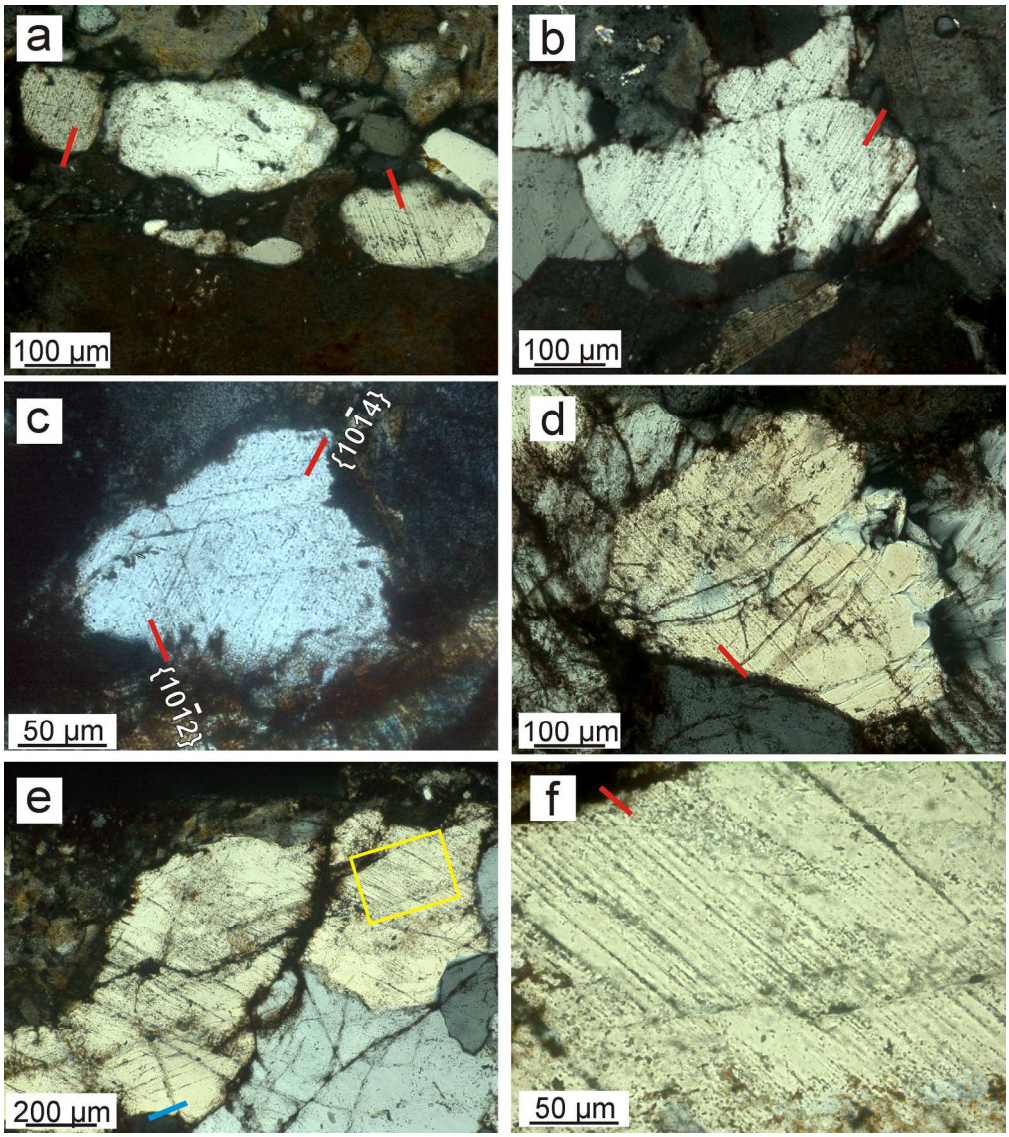

Fig. 7. Thin section microphotographs of PDFs, taken in cross polarized light. Orientation of PDFs is accentuated with the short red line. (a) Two quartz grains with one set of PDFs each, sample SHHI-2017-3 (No. 3, thin section 170353), (b) one set of PDFs in quartz, sample SHHI-2017-3 (170351). (c) two sets of PDFs of {101-4} and {101-2} orientations in quartz, sample SHHI-2017-8 (No. 8, thin section 170369), and (d) one set of PDFs in quartz, sample SHHI-2017-3 (170351). (e) One set of PDFs and PFs (orientation accentuated with the short blue line) in fragmented quartz aggregate. Yellow box highlights the area of the image (f), sample SHHI-2017-3 (170352), (f) one set of decorated PDFs, sample SHHI-2017-3 (170352). See Table 1 and Fig. 3c for descriptions and locations of samples.

191x215mm (300 x 300 DPI)

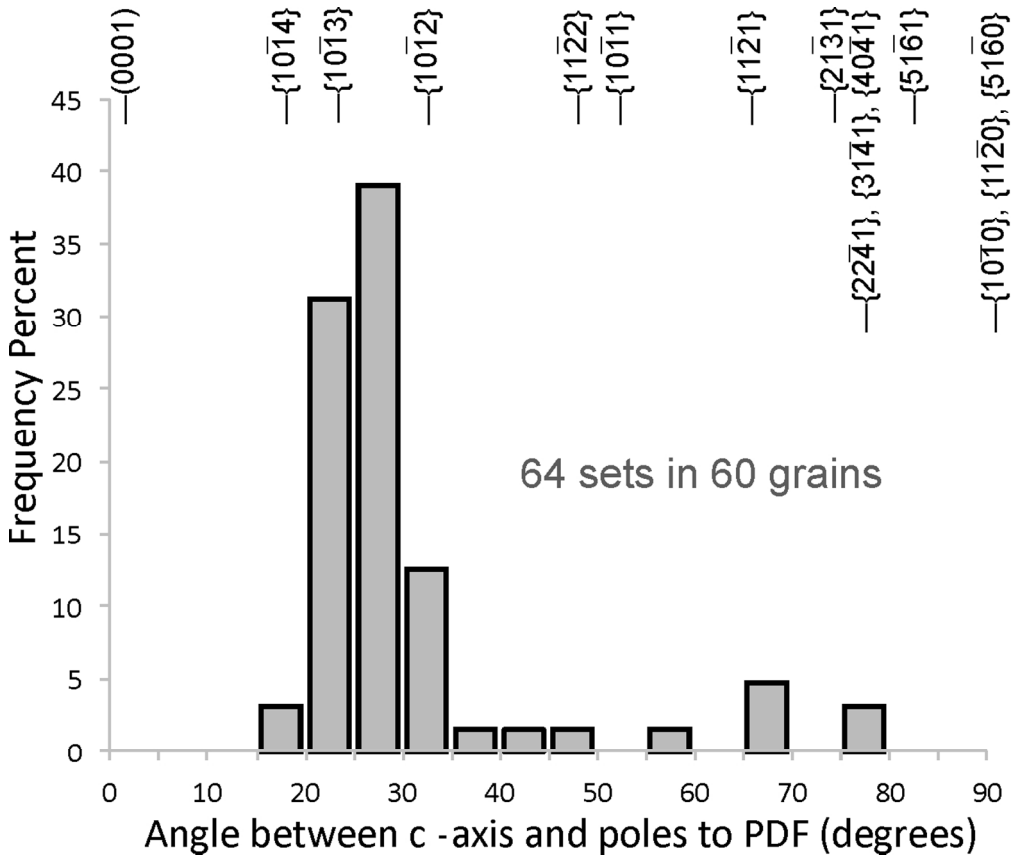

Fig. 8. Histogram of angles between c-axis and poles to PDF's in 5° bins and possibly corresponding PDF orientations.

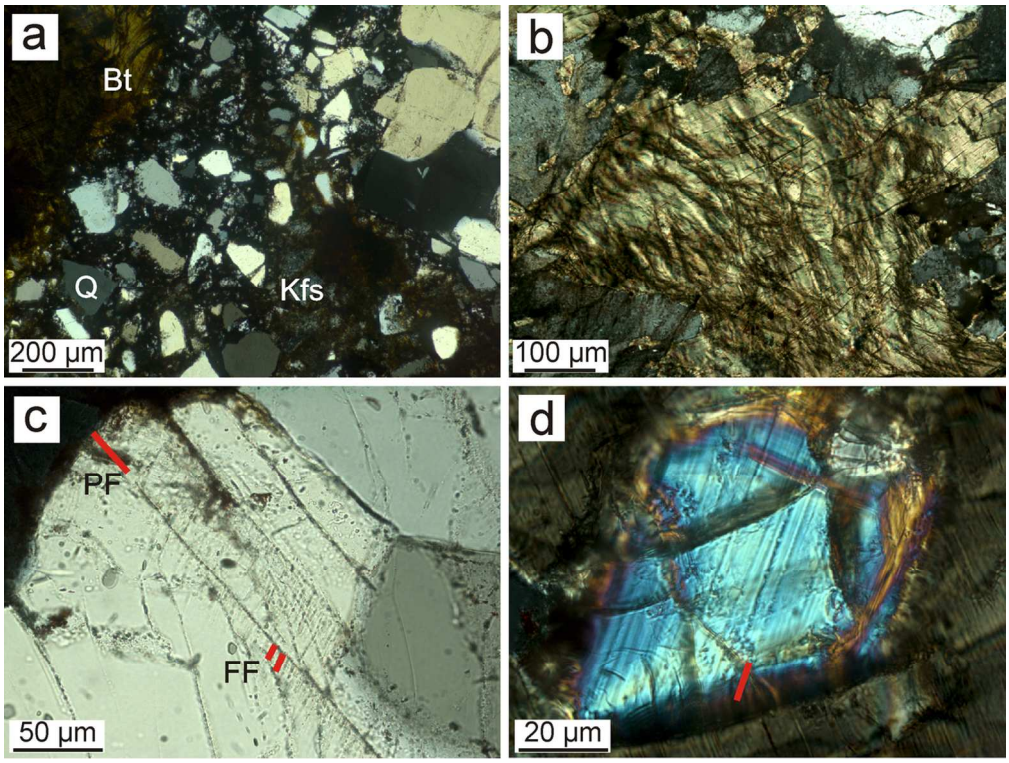

Fig. 9. Thin section microphotographs of possible shock deformation features, all images taken with crossed polarizers. (a) Brecciated vein in coarse-grained granite sample SHHI-2017-3 (No. 3, thin section 170353). Vein is filled with angular clasts of the minerals occurring in the surroundings (quartz and feldspar), (b) kink-bands in biotite, sample SHHI-2017-8 (No. 8, thin section 170369), (c) planar features and feather features in quartz, sample SHHI-2017-8 (thin section 170572), (d) possible planar microdeformations in zircon, sample SHHI-2017-8 (thin section 170571). Orientations of planar features are accentuated with short red lines. Abbreviations: Bt – biotite, Q – quartz, Kfs – potassium feldspar, PF – planar features, FF – feather features. See Table 1 and Fig. 3c for descriptions and locations of samples.

121x91mm (300 x 300 DPI)